Calculation of turbulent flow through engine inlet ports

Yeng-Yung Tsui and Shao-Yu Lee
Department of Mechanical Engineering, National Chiao Tung University, Hsinchu, Taiwan, Republic of China

The flow in an axisymmetric assembly of an engine intake port and valve is under investigation, using multidimensional analysis. The model is formulated in a curvilinear coordinate system and solved with nonstaggered grids. The turbulent effects are characterized by the k-ε model. The ε equation is modified to emphasize the effects of the normal stresses. The modification results in reduction of the turbulence and length scale in the valve passage and improves the computational accuracy for the cases considered.

Keywords: engine inlet port; turbulent flow; k-ε model; finite-volume method

Introduction

It is well recognized that the design of inlet ports and valves plays an important role in engine performance. The engine breathing capacity is usually characterized by the discharge coefficient of the port. An important parameter affecting the flow in the port/valve assembly is the valve lift. Measurements by other authors[1–3] indicated that four flow patterns exist (Figure 1). Flow at small valve lifts remains attached without separation in the valve passage (pattern 1). Because of the diminishing effect of the boundary layers, the discharge coefficient increases with lift. At a certain lift the boundary layer breaks away from the valve sealing face (pattern 2), reducing the effective flow area and, thus, the discharge coefficient. The dip in discharge coefficient is then followed by a rise with increasing lift. At higher lifts the flow also separates from the seat sealing face (pattern 3). Once this occurs, the discharge coefficient drops dramatically. Further increasing the lift, the flow reattaches on the valve sealing face (pattern 4). However, the discharge coefficient continues to decrease, but at a lower rate. The existence of the flow patterns was confirmed in reports[4,5] in which the LDA was used to measure radial velocity at the exit of the valve passage.

An effective means to improve flow characteristics is to round off the sharp corners on the valve and seat sealing faces.[1–5] With the minor modification, the flow separation in the valve passage is delayed and a direct transition from flow pattern 1 to pattern 4 exists. The improvement in discharge coefficient could be 15–30 percent.

In the previous studies[4,5] the flow structure was examined in detail only at the exit of the valve passage. To fully understand the way in which the flow develops, it is necessary to study the flow inside the port and valve passage. In the study of Isshiki *et al.*[6] numerical technique was adopted to model the three-dimensional steady flow in a number of intake port configurations. The accuracy of prediction had only been assessed by comparing it with the measured discharge coefficient. A discontinuity was shown in the experimental curve of discharge coefficient against lift, indicating flow breakaway in the valve passage at medium-to-high lifts. But this is not observed in the predictions. Tindal *et al.*[7] used LDA to investigate steady flow in an axisymmetric port and a helical port with sharp-edge sealing faces. Their results confirmed the existence of the four flow modes at different valve lifts. The results for the axisymmetric case had been used to assess numerical calculations in the study by Demirdzic *et al.*[8] There was fair agreement between the measurements and the mean flow predictions, but underprediction of turbulence intensity was substantial. In the studies of Gosman and Ahmed[9] and Ahmed[10] both the HWA and multidimensional analysis were used to investigate the flow in an axisymmetric port with rounded corners on sealing faces. As expected, flow separation occurs in the experiments when the valve lift is sufficiently high. However, the separation was not found in the calculations. Besides, compared with mean flow, the turbulence prediction is less satisfactory. In the calculations of Demirdzic *et al.*[8] and Gosman and Ahmed[9] the standard k-ε turbulence model was used. This implies that the standard k-ε model is not adequate for such flows in the intake port.

In this study a numerical procedure employing body-fitted nonorthogonal, nonstaggered grids is adopted to examine the steady flow in an axisymmetric assembly of port and valve.

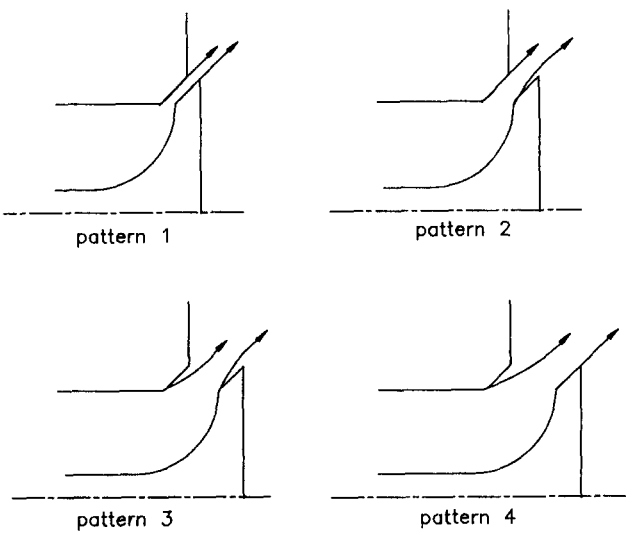

Figure 1 Flow patterns in the valve passage

Address reprint requests to Professor Tsui at the Department of Mechanical Engineering, National Chiao Tung University, Hsinchu 30049, Taiwan, Republic of China.

Received 20 August 1991; accepted 7 January 1992

The ε equation of the k-ε model is modified to emphasize the effects of the normal stresses on the production of turbulent dissipation. Two configurations are considered: one with sharp corners and the other with rounded corners on the sealing faces. The predictions by the standard k-ε model as well as the modified model are compared with the data of Gosman and Ahmed[9] and Bicen *et al.*[4]

Mathematical model and solution procedure

Equations of motion

To cope with the complex geometries in the assembly of port, valve, and cylinder, the equations are written in curvilinear nonorthogonal coordinates:

Conservation of mass

$$\frac{1}{\mathrm{Jr}}\left[\frac{\partial G_1}{\partial \xi}+\frac{\partial G_2}{\partial \eta}\right]=0 \tag{1}$$

Conservation of momentum in the z-direction

$$\begin{aligned}&\frac{1}{\mathrm{Jr}}\left[\frac{\partial}{\partial \xi}(G_1 u)+\frac{\partial}{\partial \eta}(G_2 u)\right]\\&\quad=-\frac{1}{\mathrm{J}}(r_\eta p_\xi - r_\xi p_\eta)+\frac{1}{\mathrm{Jr}}\frac{\partial}{\partial \xi}\left\{\frac{r\mu_{\mathrm{eff}}}{\mathrm{J}}[(2r_\eta^2+z_\eta^2)u_\xi\right.\\&\qquad\left.-(2r_\xi r_\eta+z_\xi z_\eta)u_\eta-(z_\eta r_\eta v_\xi - z_\eta r_\xi v_\eta)]\right\}\\&\qquad+\frac{1}{\mathrm{Jr}}\frac{\partial}{\partial \eta}\left\{\frac{r\mu_{\mathrm{eff}}}{\mathrm{J}}[(2r_\xi^2+z_\xi^2)u_\eta-(2r_\xi r_\eta+z_\xi z_\eta)u_\xi\right.\\&\qquad\left.+(z_\xi r_\eta v_\xi+z_\xi r_\eta v_\eta)]\right\}\end{aligned} \tag{2}$$

Conservation of momentum in the r-direction

$$\begin{aligned}&\frac{1}{\mathrm{Jr}}\left[\frac{\partial}{\partial \xi}(G_1 v)+\frac{\partial}{\partial \eta}(G_2 v)\right]\\&\quad=-\frac{1}{\mathrm{J}}(z_\xi p_\eta - z_\eta p_\xi)+\frac{1}{\mathrm{Jr}}\frac{\partial}{\partial \xi}\left\{\frac{r\mu_{\mathrm{eff}}}{\mathrm{J}}[(2z_\eta^2+r_\eta^2)v_\xi\right.\\&\qquad\left.-(2z_\xi z_\eta+r_\xi r_\eta)v_\eta+(r_\eta z_\xi u_\eta - r_\eta z_\eta u_\xi)]\right\}\\&\qquad+\frac{1}{\mathrm{Jr}}\frac{\partial}{\partial \eta}\left\{\frac{r\mu_{\mathrm{eff}}}{\mathrm{J}}[(2z_\xi^2+r_\xi^2)v_\eta-(2z_\xi z_\eta+r_\xi r_\eta)v_\xi\right.\\&\qquad\left.-(r_\xi z_\xi u_\eta+r_\xi z_\eta u_\xi)]\right\}-2\mu_{\mathrm{eff}}\frac{v}{r^2}\end{aligned} \tag{3}$$

In the above equations z and r are the coordinates in axial and radial directions (Figure 2), u and v are the mean velocities in the z- and r-directions, respectively, ξ and η represent the system of general coordinates, G_1 and G_2 denote the mass flow rates across the η and ξ coordinates, respectively, and are expressed as

$$G_1 = r\rho r_\eta u - r\rho z_\eta v \tag{4}$$

$$G_2 = r\rho z_\xi v - r\rho r_\xi u \tag{5}$$

The symbol J represents the Jacobian of transformation. The effective viscosity μ_{eff} is the sum of kinematic and eddy viscosities.

Turbulence modeling

The standard k-ε model calculates the eddy viscosity from

$$\mu_t = \mathrm{C}_\mu \frac{\rho \mathrm{k}^2}{\varepsilon} \tag{6}$$

Notation

C_1, C_2, C_3, C_μ	Constants for turbulence model
C_D	Discharge coefficient
D	Port diameter
D, E	Coefficients of the pressure difference terms in the momentum equations
G_1, G_2	Mass fluxes across η and ξ coordinates, respectively
$H(u_c)$, $H(v_c)$	Difference representations of the convective and diffusive fluxes of momentum
J	Jacobian of transformation
k	Turbulent kinetic energy
L^*	Ratio of valve life to port diameter
p	Pressure
P_k, P_ε	Productions of turbulent energy and dissipation rate, respectively
P_{kn}, P_{ks}	Productions of turbulent energy due to normal stresses and shear stresses, respectively
Q	Inlet velocity
S_u, S_v	Source terms related to the u and v momentum equations, respectively
u, v	Velocities in the z- and r-directions, respectively
U	Magnitude of resultant velocity
z, r	Axial and radial coordinates, respectively

Greek symbols

α	Flow angle
ε	Turbulent dissipation rate
μ_{eff}	Effective viscosity
μ_t	Eddy viscosity
ρ	Density
σ_k, σ_ε	Turbulent Prandtl numbers for k and ε, respectively
ξ, η	Curvilinear coordinates

Superscripts

	Corrected values
	Interpolated values

Subscripts

e, w, n, s	Values associated with cell face points
E, W, N, S	Values associated with neighboring nodal points
ne, nw, se, sw	Values associated with cell vertices
P	Pertaining to the main nodal point
u, v	Associated with the u and v momentum equations

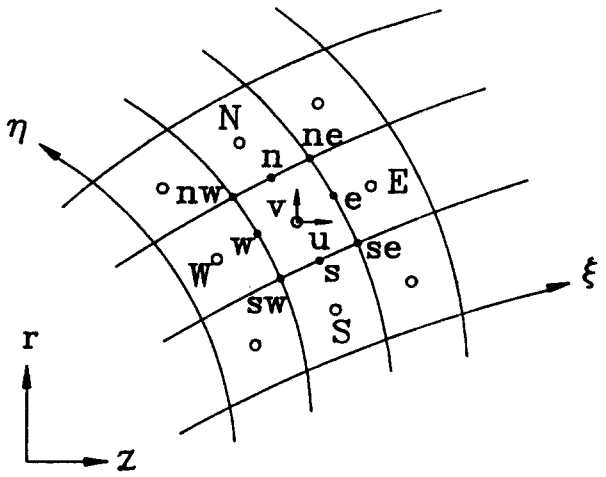

Figure 2 Illustration of a control volume surrounding a node P

where k is the turbulent kinetic energy, ε is its dissipation rate, and C_μ is taken as a constant. The transport equations for the k and ε in the general coordinates are

$$\frac{1}{Jr}\left[\frac{\partial}{\partial\xi}(G_1 k)+\frac{\partial}{\partial\eta}(G_2 k)\right] = \frac{1}{Jr}\frac{\partial}{\partial\xi}\left\{\frac{r\mu_{eff}}{J\sigma_k}[(r_\eta^2+z_\eta^2)k_\xi-(r_\xi r_\eta+z_\xi z_\eta)k_\eta]\right\} + \frac{1}{Jr}\frac{\partial}{\partial\eta}\left\{\frac{r\mu_{eff}}{J\sigma_k}[(r_\xi^2+z_\xi^2)k_\eta-(r_\xi r_\eta+z_\xi z_\eta)k_\xi]\right\} + P_k-\rho\varepsilon \tag{7}$$

$$\frac{1}{Jr}\left[\frac{\partial}{\partial\xi}(G_1\varepsilon)+\frac{\partial}{\partial\eta}(G_2\varepsilon)\right] = \frac{1}{Jr}\frac{\partial}{\partial\xi}\left\{\frac{r\mu_{eff}}{J\sigma_\varepsilon}[(r_\eta^2+z_\eta^2)\varepsilon_\xi-(r_\xi r_\eta+z_\xi z_\eta)\varepsilon_\eta]\right\} + \frac{1}{Jr}\frac{\partial}{\partial\eta}\left\{\frac{r\mu_{eff}}{J\sigma_\varepsilon}[(r_\xi^2+z_\xi^2)\varepsilon_\eta-(r_\xi r_\eta+z_\xi z_\eta)\varepsilon_\xi]\right\} + P_\varepsilon-C_2\rho\frac{\varepsilon^2}{k} \tag{8}$$

where P_k and P_ε designate the productions of k and ε, respectively,

$$P_k=\frac{\mu_t}{J^2}(u_\eta z_\xi-u_\xi z_\eta+v_\eta r_\xi-v_\xi r_\eta)^2 + \underline{\frac{\mu_t}{J^2}\left\{2(u_\xi r_\eta-u_\eta r_\xi)^2 + 2(v_\eta z_\xi-v_\xi z_\eta)^2+2J^2\left(\frac{v}{r}\right)^2\right\}} \tag{9}$$

$$P_\varepsilon=C_1P_k\frac{\varepsilon}{k} \tag{10}$$

The empirical constants in the standard k-ε model are given as[11] $C_\mu=0.9$, $\sigma_k=1.0$, $\sigma_\varepsilon=1.3$, $C_1=1.44$, and $C_2=1.92$.

Although the standard k-ε model has been successful in calculating a variety of flows, it is not without deficiencies. Leschziner and Rodi[12] showed that with some modifications of the model to account for either the effects of streamline curvature on turbulence or the preferential influence of normal stresses on the turbulence dissipation, the recirculating flows in an annular jet and a plane jet are better predicted. For flows with an adverse pressure gradient Rodi and Scheuerer[13] found that the predicted dissipation is too small, giving rise to too large shear stresses near the wall. This indicates that a modification of the ε equation is necessary. Hanjalic and Launder[14] pointed out that energy transfer across the spectrum is promoted by normal stresses. Such an effect can be achieved by enhancing ε through modifying the production term of the ε equation as follows

$$P_\varepsilon=(C_1P_{ks}+C_3P_{kn})\frac{\varepsilon}{k} \tag{11}$$

Here P_{ks} denotes the production part involving shear stresses and P_{kn} the part involving normal stresses. To account for the preferential effects of normal stress, a value of C_3 larger than the constant C_1 should be employed. Different expressions for P_{kn} and different values for C_3 have been reported.[12–14] In the present study P_{ks} simply represents the first term on the right-hand side of Equation 9 and P_{kn} the last term being underlined. The selection of C_3 is based on the optimization test on the cases considered in the following section.

Boundary conditions

For the case with rounded corners the inlet velocities and turbulent energy are taken from the measurements of Ahmed.[10] As for the sharp-corner configuration, the required distributions of velocity and turbulence are obtained through extrapolation from the rounded-corner case. The velocity and turbulence profiles are similar to those used in the rounded-corner one, but the magnitudes are enlarged by a factor equal to the ratio of the mass fluxes through the two ports. The dissipation rate at inlet is calculated from the k distribution and a step formulation for the dissipation length scale. Since the computational domain is chosen such that the outlet boundary is located far from the exit of the port (at a distance of 25 diameters of the port), the flow at outlet boundary is expected to be parallel to the wall and, thus, the streamwise gradients of all variables are set to zero. On the solid boundaries, the wall function is used to bridge the near wall region.[11] At the axis of symmetry the normal gradients of all variables are set to zero except that the velocity v, being normal to the axis, itself is zero.

Numerical solution procedure

The discretization is performed in the physical space following a finite volume approach. The nonstaggered grid arrangement is used in which all variables, including the velocity components u and v, are located at the center of each control volume, as shown in Figure 2. The difference equations are obtained by taking integration of the governing equations over a control volume. Convective terms are approximated by the upwind differencing scheme and diffusive terms by the central differencing scheme. It is known that the upwind scheme inherently has the problem of numerical diffusion. The resultant artificial viscosity may overshadow the true viscosity of turbulence modeling. One way to alleviate the problem is to use higher order schemes, such as the QUICK scheme[15] and the linear upwind scheme.[16] However, high order schemes may cause oscillation[17] in velocity unless special treatments are made. An alternative way is to use fine enough grid to diminish numerical diffusion. Grid refinement test has shown that the grid used in this study, which is described later, is adequate to

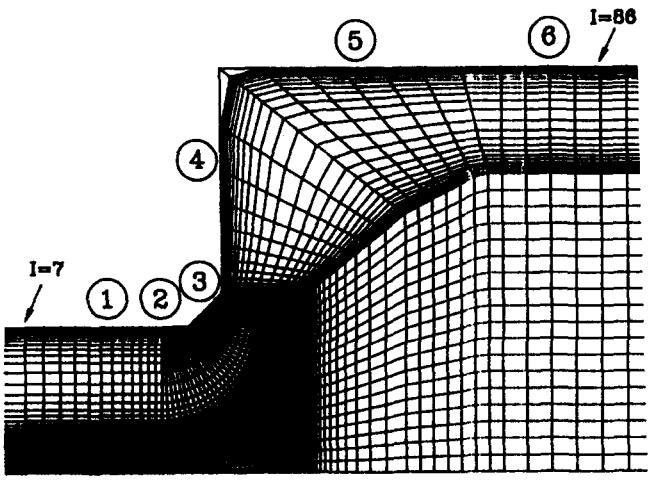

Figure 3 A typical grid arrangement for the case with sharp corners

suppress numerical diffusion. It is also well known that with the use of nonstaggered grid it may lead to pressure-velocity decoupling[18] and, thus, oscillatory solutions. To overcome this problem a special interpolation procedure to calculate the cell-face velocities has been proposed by Rhie and Chow[19] and extensively tested by Peric.[20] This method is briefly described in the Appendix.

Computational grids

To ensure accuracy of the calculation, the computational grid should be boundary fitted and have sufficient resolution in regions of interest. For the port/cylinder assembly considered in the present study, the solution domain is first divided into six zones numbered 1–6 (Figure 3). Each zone is bounded by the discontinuities in the upper and/or lower boundaries (part of the first zone and part of the sixth zone are truncated in Figure 3). In each zone a simple transfinite mapping method[21] was used to generate the grid system. Grid dependence studies have been conducted, and a grid with 148 × 48 nodal points was shown to be adequate.[22] The grid contains 64*29 nodes in the port duct and valve passage, which is similar to the one used by Gosman and Ahmed[9,10] and was also shown to yield grid-independent solutions.[10] An example of the grid for the sharp-corner case is portrayed in Figure 3.

Results and discussion

Test case I with rounded corners

The first case tested is the one investigated by Gosman and Ahmed.[9,10] The corners on the sealing faces at the entrance of the valve passage are rounded off. The details of the arrangement are shown in Figure 4a. Five different valve lifts have been studied: $L^* = 0.05$, 0.10, 0.15, 0.20, and 0.25, where L^* is the ratio of the valve lift to the port diameter (= 102.6 mm).

Before discussing the results, Figure 5 is presented to illustrate the effects of C_3 on the predictions. The test bench used is the case with $L^* = 0.25$. Three different values, 2.0, 3.0, and 4.4, along with the standard value, 1.44, have been tested. The resulted profiles of velocity (Q/U in the figure, where Q is the velocity magnitude and U the mean velocity at inlet), flow angle (α, which is defined with respect to the valve axis), and turbulent kinetic energy at the inlet of the valve passage are shown. It is apparent that for the values other than 1.44 the mean velocities are nearly identical and only slight differences exist between the predictions of turbulence. Similar results can be found at other locations. According to our experience, the use of 4.44 may cause divergence in some cases and sometimes it is difficult to converge with 2.0. Thus, the value of 3.0 is adopted in the present study.

It could be observed from results[22] that at low lifts ($L^* = 0.05$, 0.1, and 0.15) the predictions by the standard k-ε model (SKE) and the modified k-ε model (MKE) show similar flow patterns, with flow remaining attached in the valve passage. When the lift increases to 0.20, the flow starts to break away from the seat sealing face in the MKE results, but not in the calculations of SKE. Further increase of L^* to 0.25 leads to enlargement of the separation zone. However, the flow predicted by the SKE remains attached. This difference can be identified in Figure 6, which displays the streamlines and the velocity vectors in the valve passage calculated using the two models. In the figure the stream functions are normalized by the mass flow rate. It is also of interest that a separation bubble exists in the MKE predictions in the curved region near the

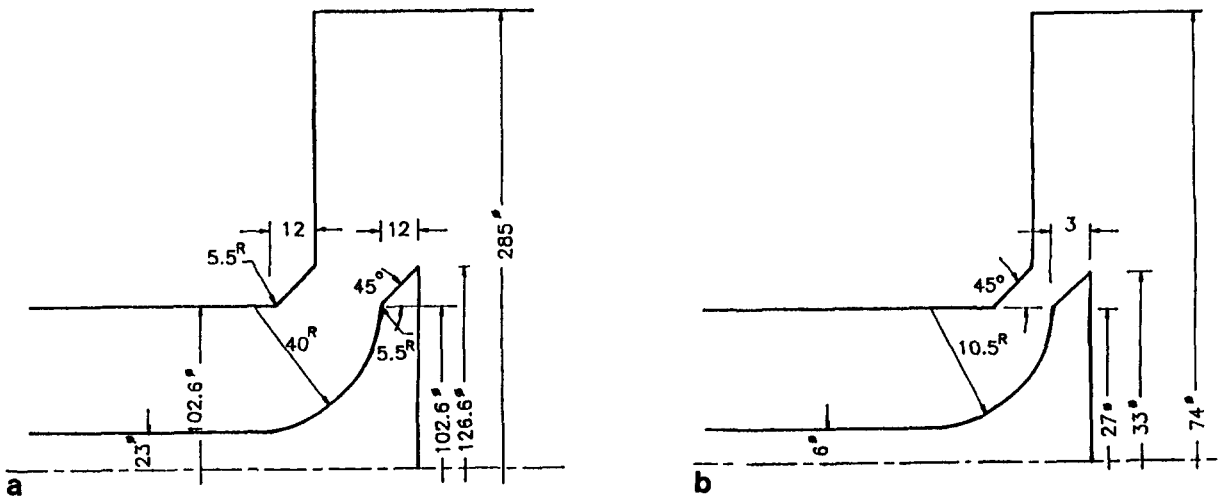

Figure 4 Details of the assemblies: (a) case I with rounded corners; (b) case II with sharp corners

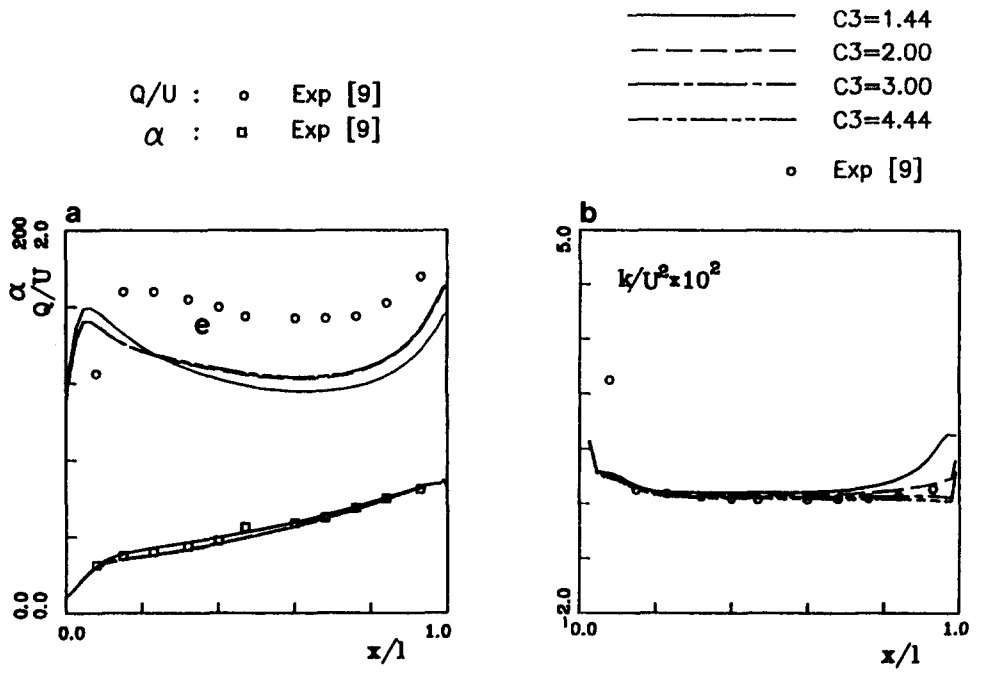

Figure 5 Sensitivity test for C_3: (a) magnitude and flow angle of resultant velocity; (b) turbulent kinetic energy

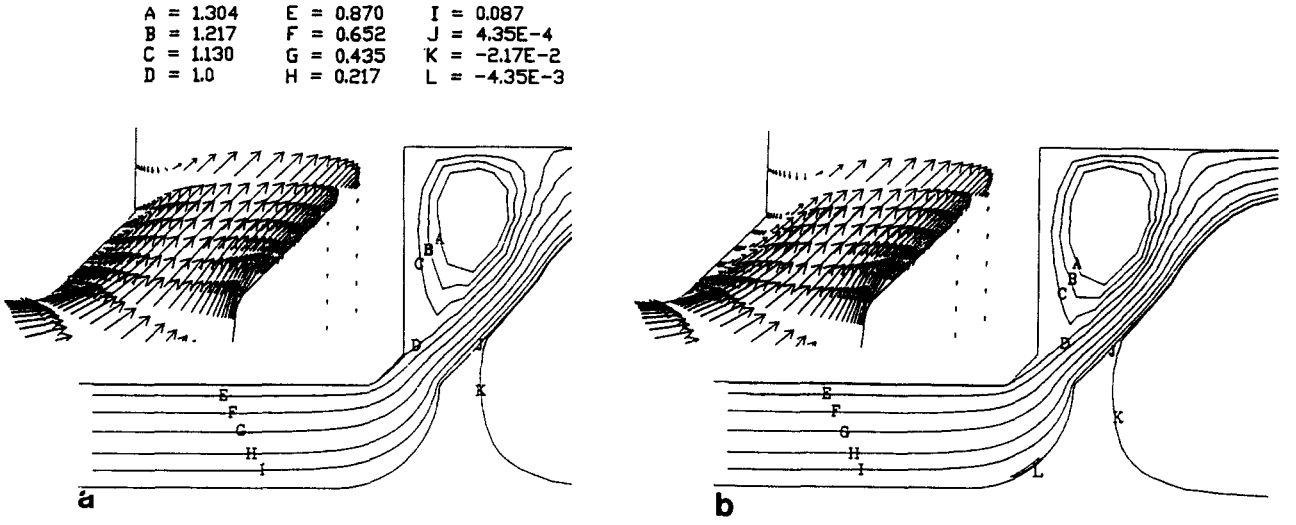

Figure 6 Predicted streamlines and velocity vectors for rounded-corner case with $L^* = 0.25$: (a) SKE; (b) MKE

valve head, as shown in the streamline plot (Figure 6b). Because the flow is directed toward the cylinder head, a high pressure regime is formed at the head. Thus, the flow is retarded due to the adverse pressure gradient along the wall of the valve stem. This flow separation was confirmed in the experimental study of Gosman and Ahmed.[9]

Comparisons of the mean flow and turbulence characteristics between the predictions and measurements are given in Figures 7 and 8 for the lifts of 0.10 and 0.25, respectively. The profiles of the flow properties are plotted at three transverse stations as indicated in Figures 7a and 8a: station A is located 25 mm ahead of the cylinder head, station B is located 4 mm (normal distance) downstream of the inlet of the valve passage, and station C is just at the exit of the passage. More comparisons can be found elsewhere.[22] It is noted that, as pointed out by Gosman and Ahmed,[9] the data measured by the HWA are not reliable in and near zones of separated flow. These regions are indicated by a dashed line in the plots. Besides, the accuracy of the data is also limited close to walls. For the case of lower lift the predictions by the two models will reproduce the measured flow velocities (Figure 7a). For the higher lift case both models underpredict the velocities at stations B and C (Figure 8a). The underprediction is more serious for the SKE model because no flow separation appears, as observed in Figure 6. The difference between the measurements and the MKE predictions reveals that the underprediction of the size of the separation zone is not small. Comparison of turbulent energy for the two cases is illustrated in Figures 7b and 8b,

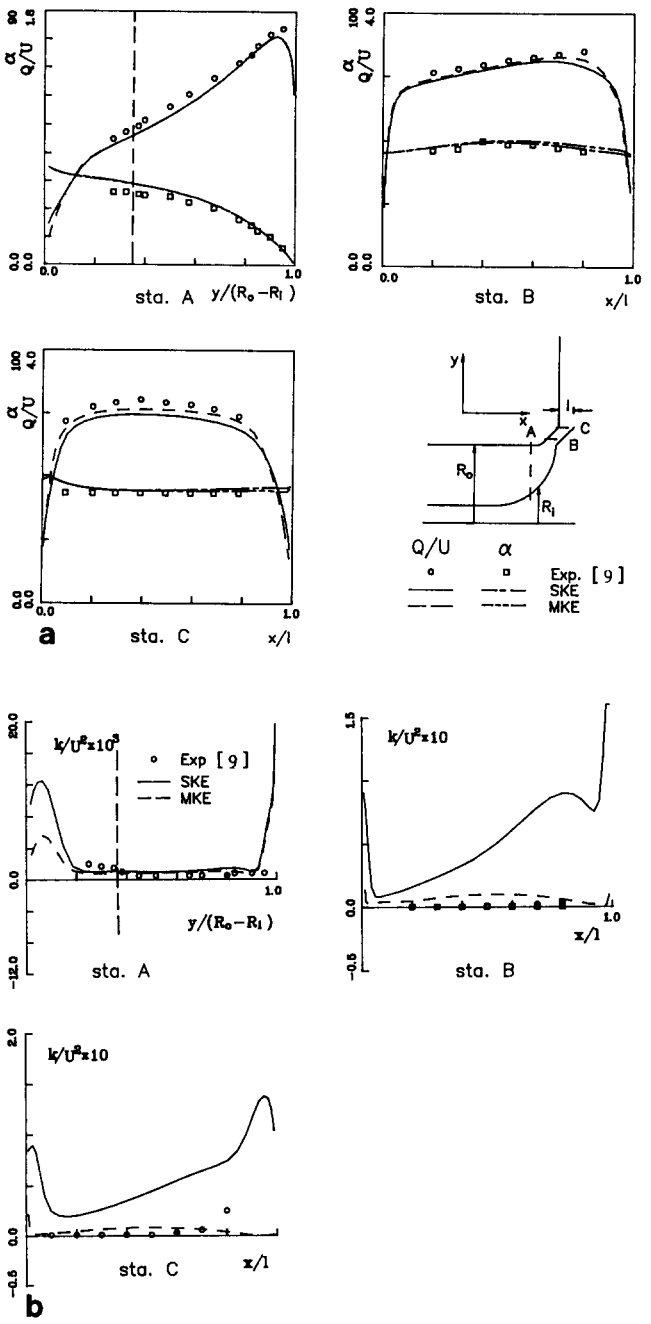

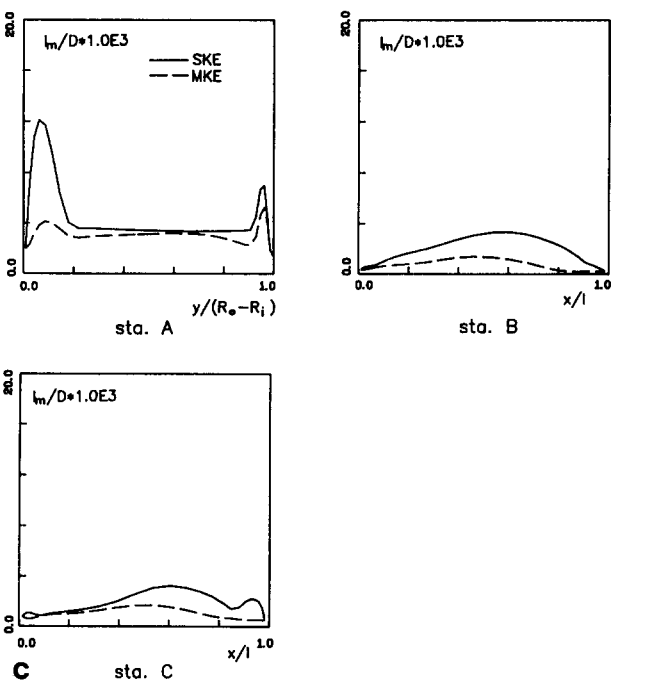

Figure 7 Comparison between predictions and measurements for rounded-corner case with $L^* = 0.10$: (a) magnitude and flow angle of resultant velocity; (b) turbulent kinetic energy; (c) turbulent length scale

respectively. At station A the agreement between predictions and experimental data is good. The lower level of turbulent energy near the valve head for the MKE is attributed to the fact that the curved streamlines there augment the turbulence dissipation through the normal stress part in Equation 9. This effect spreads down and over the entire valve passage, as seen at stations B and C. This is also reflected in the calculation of length scale shown in Figures 7c and 8c. The length scale predicted by the MKE is smaller than that by the SKE, especially in the region near the valve and in the passage. It is noted from Figure 8b that the predicted turbulence in the separation zone and the near region at stations B and C is much lower than the measurements. However, it should be recalled that the accuracy of the measurements are questionable in these regions. This uncertainty should be more serious at the exit of the valve passage because the size of the separation zone is the largest there.

The predicted discharge coefficients along with experimental data are displayed in Figure 9. In the region of low-to-medium lifts the predictions follow the trend that the discharge coefficient gradually increases with the lift. The SKE prediction is slightly better than that of MKE. As the lift increases beyond 0.20, the experimental curve as well as the MKE prediction at $L^* = 0.25$ decline sharply, while that of the SKE decrease only slightly due to its failure to produce flow separation.

Test case II with sharp corners

The second case was studied in references 4 and 5 in which the LDA was used to measure the flow velocity. The configuration of the port and valve is shown in Figure 4b. The major difference from the first case is the sharp corners on the sealing faces, apart from the size. Four different lifts, corresponding to the four flow modes described in the section of introduction, have been tested: $L^* = 0.074$, 0.157, 0.222, and 0.296.

The plots of velocity vector in the valve passage for the different lifts are shown in Figure 10. At the lowest lift the flow attaches on both sealing faces in the SKE results, whereas a thin separation layer adjacent to the valve crown appears in the calculations of MKE. As the lift is increased to 0.157, the flow breaks away from the valve face in both predictions. When the lift is further increased, the flow also separates on the seat sealing face in both results. At the highest lift the zone of separation on the seat face is enlarged while that on the valve face diminishes. Generally, the flow structure agrees with the flow patterns discussed in the introduction. The flow field data available for comparison is the radial velocity at a station 0.5 mm above the exit plane of the passage for the three higher lift cases. It is obvious from Figure 11 that the predictions are improved by the MKE model, although the size of the separation zone and, thus, the velocity are still underpredicted.

In Figure 12 the predicted and measured discharge coefficients are compared. In general, as expected, the MKE

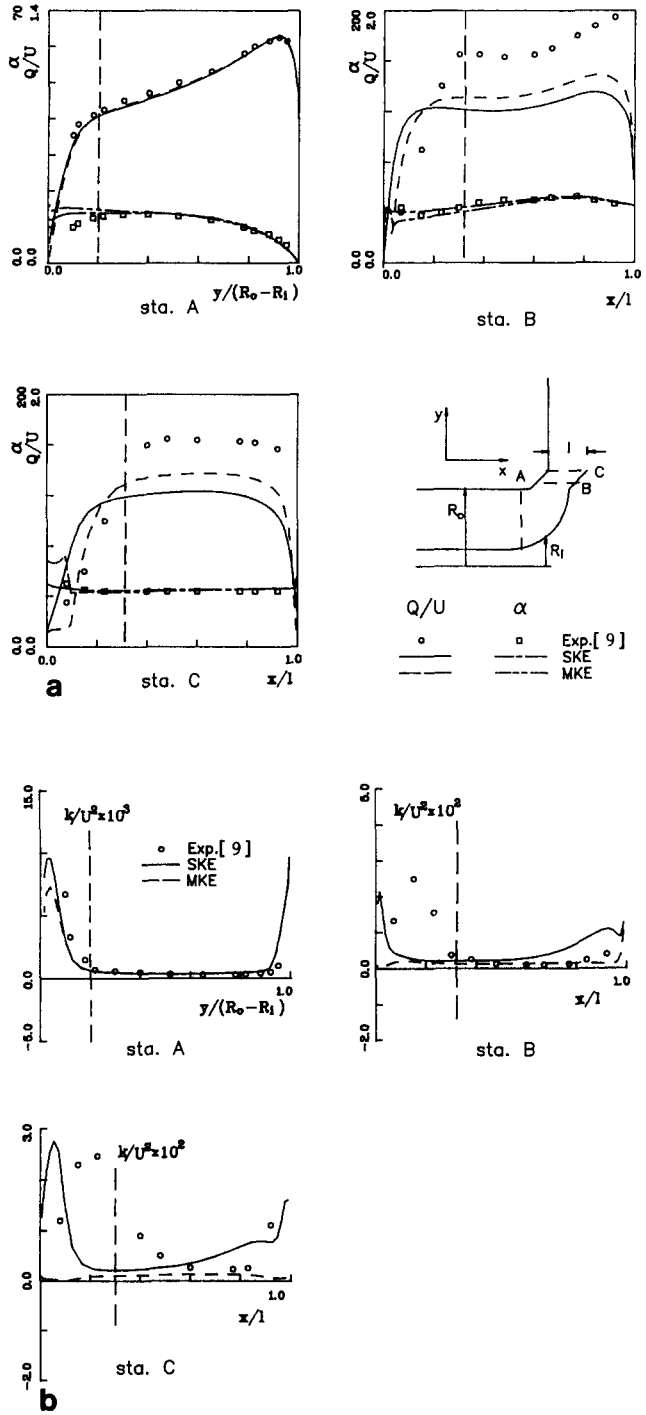

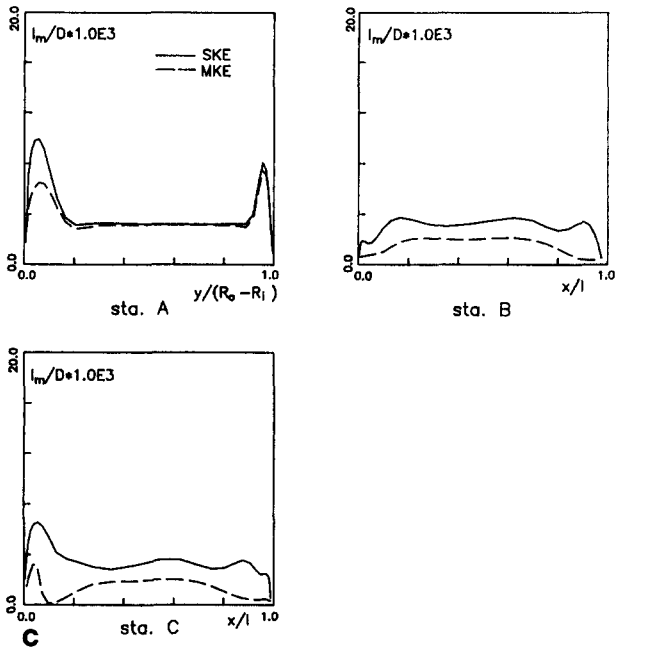

Figure 8 Comparison between predictions and measurements for rounded-corner case with $L^* = 0.25$: (a) magnitude and flow angle of resultant velocity; (b) turbulent kinetic energy; (c) turbulent length scale

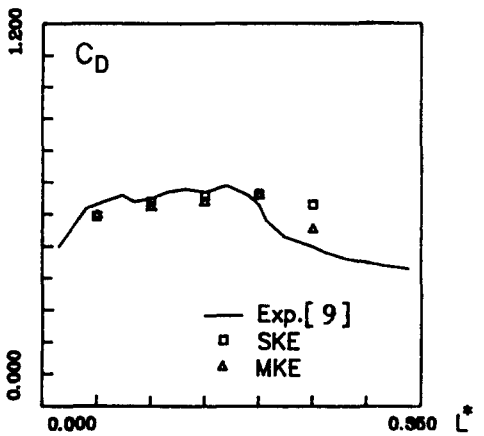

Figure 9 Comparison between predicted and measured discharge coefficients for rounded-corner case

model performs better than the SKE model. The slightly poorer performance of the MKE at the lowest lift implies that the thin separation layer observed in Figure 10 may not be plausible.

The predicted discharge coefficients by the MKE and the experimental data for the two cases presented above are redepicted in Figure 13. An additional set of prediction data related to sharp corners but with lifts the same as those used in the rounded-corners case are added to the figure. It is clear that without rounding the corners the discharge coefficient is reduced. This is, of course, attributed to the block effects of separation in the passage.

Conclusions

A model for steady flow in an axisymmetric assembly of port and valve is developed. The model is formulated in a curvilinear coordinate system and solved with a nonstaggered grid arrangement. The standard k-ε model together with a preferential k-ε model, in which the ε equation is modified to be sensitized to the normal stresses, are tested on two different port configurations.

For the case with rounded corners the modified model produces flow separation at seat sealing face when the lift is large enough, whereas the standard model does not. The failure to predict such a feature represents a major deficiency of the standard k-ε model. It is shown that the turbulent energy and

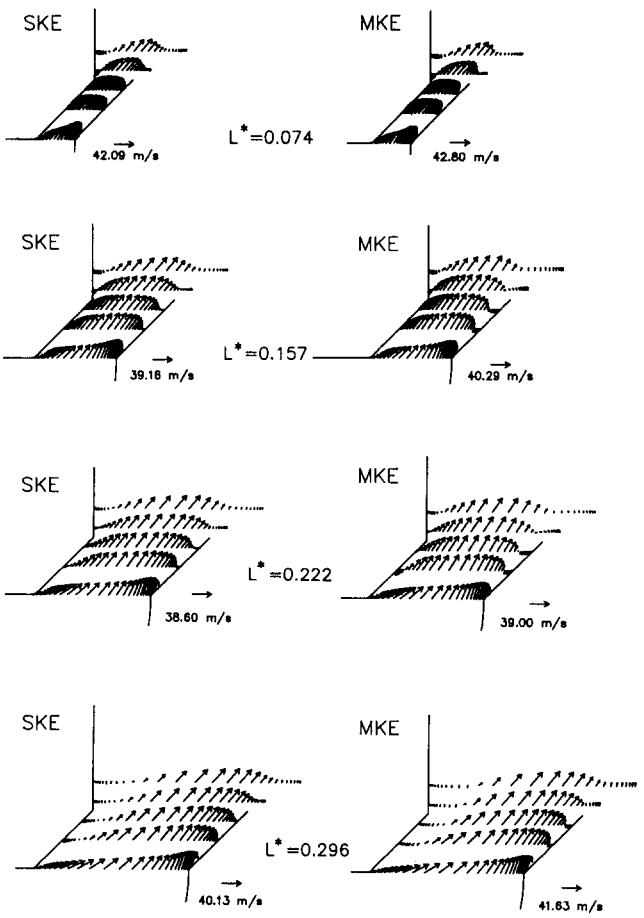

Figure 10 Predicted velocity vectors in the valve passage for sharp-corner case

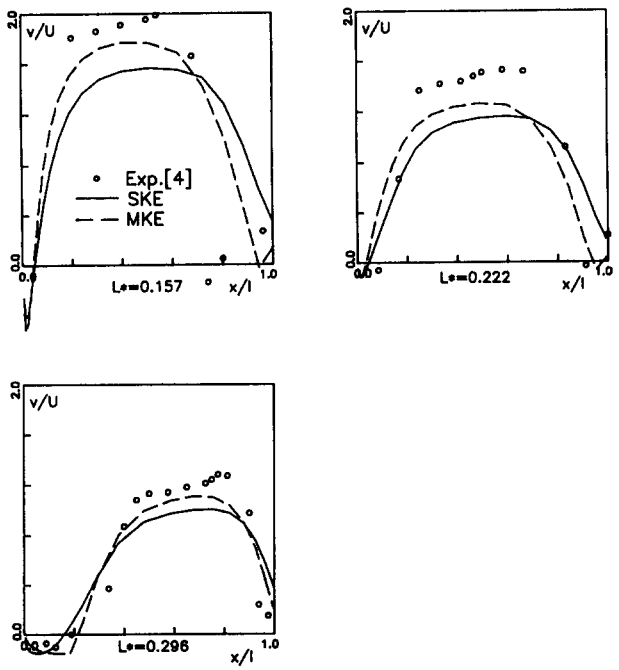

Figure 11 Comparison of radial velocity at the exit of the valve passage between predictions and measurements

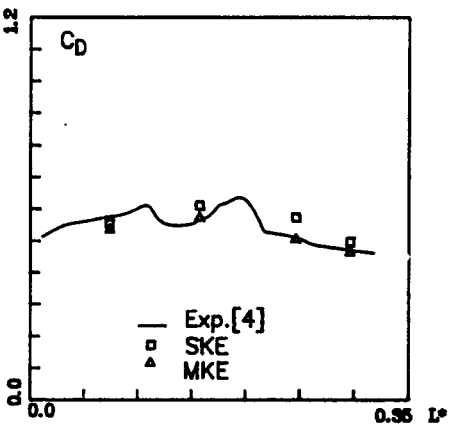

Figure 12 Comparison between predicted and measured discharge coefficients for sharp-corner case

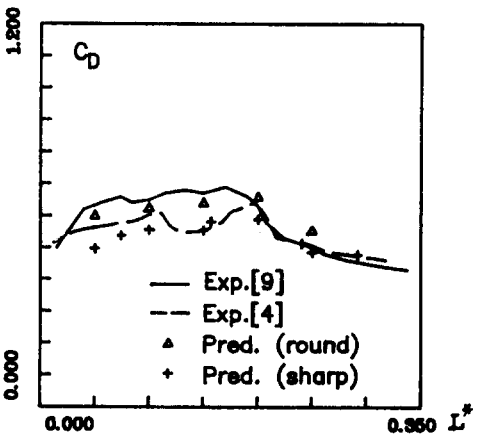

Figure 13 Comparison of discharge coefficient between the MKE predictions and measurements

length scale are reduced by the modified model when the streamlines of the flow are curved.

Without rounding off the corners, different kinds of flow separation at different lifts could be identified by both models. This indicates that with minor changes in geometry the effects on the flow field could be significant and are reflected in the calculations. Comparison with measurements reveals that the modified model performs better than the standard model.

Comparison of discharge coefficient between predictions and measurements shows that the general trend of flow variation could be obtained by the modified model. However, details of the flow features, e.g., the size of the separation zone, could not be predicted accurately.

References

1 Tanaka, K. Air flow through suction valve of conical seat. *Aeronautical Research Institute Report*, Tokyo Imperial University, Japan, 1929, 260 and 361

2 Wood, G. B., Hunter, D. U., Taylor, E. S. and Taylor, C. F. Airflow through intake valves. *Trans. SAE*, 1942, **50**, 212

3 Kastner, L. J., Williams, T. J. and White, J. B. Poppet inlet valve characteristics and their influence on the induction process. *Proc. I. Mech. Eng.*, 1963, **178**, 955–975

4 Bicen, A. F., Vafidis, C. and Whitelaw, J. H. Steady and unsteady

airflow through the intake valve of a reciprocating engine. *ASME J. Fluids Eng.*, 1985, **107**, 413–420
5 Vafidis, C. and Whitelaw, J. H. Steady and pulsating air flow through a stationary intake valve of a reciprocating engine. *Mech. Eng. Dept. Report FS/84/4*, Imperial College, UK, 1984
6 Isshiki, Y., Shimamoto, Y. and Wakisaka, T. Numerical prediction of effect of intake port configurations on the induction swirl intensity by three-dimensional gas flow analysis. *Proc. Int. Symp. on Diagnostics and Modelling of Combustion in Reciprocating Engines*, Tokyo, Japan, 1985
7 Tindal, M. J., Cheung, R. S. and Yianneskis, M. Velocity characteristics of steady flows through engine inlet ports and cylinders. *SAE* Paper 880383, 1983
8 Demirdzic, I., Peric, M. and Yianneskis, M. Numerical predictions of the mean flow and turbulence in an axisymmetric port and their assessment against experimental data. *Proc. XIXth Int. Symp. on Heat and Mass Transfer in Gasoline and Diesel Engines*, Dubrovnik, Yugoslavia, 1987
9 Gosman, A. D. and Ahmed, A. M. Y. Measurement and multidimensional prediction of flow in an axisymmetric port/valve assembly. *SAE* Paper 870592, 1987
10 Ahmed, A. M. Y. Investigation of the flow in an idealized inlet port/poppet valve assembly. Ph.D. thesis, University of London, UK, 1987
11 Launder, B. E. and Spalding, D. B. The numerical calculation of turbulent flows. *Comp. Meth. Appl. Mech. Eng.*, 1974, **3**, 269–289
12 Leschziner, M. A. and Rodi, W. Calculation of annular and twin parallel jets using various discretization schemes and turbulence-model variations. *ASME J. Fluids Eng.*, 1981, **103**, 352–360
13 Rodi, W. and Scheuerer, G. Scrutinizing the k-ε turbulence model under adverse pressure gradient conditions. *ASME J. Fluids Eng.*, 1986, **108**, 174–179
14 Hanjalic, K. and Launder, B. E. Sensitizing the dissipation equation to irrotational strains. *ASME J. Fluids Eng.*, 1980, **102**, 34–40
15 Leonard, B. P. A stable and accurate convective modelling procedure based on quadratic upstream interpolation. *Comp. Meth. Appl. Mech. Eng.*, 1978, **19**, 59–98
16 Price, H. S., Varga, R. S. and Warren, J. E. Applications of oscillation matrices to diffusion-correction equations. *J. Math. Phys.*, 1966, **45**, 301–311
17 Tsui, Y.-Y. A study of upstream-weighted high-order differencing for approximation to flow convection. *Int. J. Numer. Methods Fluids*, 1991, **13**, 167–199
18 Patankar, S. V. *Numerical Heat Transfer and Fluid Flow*. Hemisphere, Washington, DC, 1980
19 Rhie, C. M. and Chow, W. L. A. A numerical study of the turbulent flow past an isolated airfoil with trailing edge separation. *AIAA* Paper 82-0998, 1982
20 Peric, M. A finite volume method for prediction of three-dimensional fluid flow in complex ducts. Ph.D. thesis, University of London, UK, 1985
21 Demirdzic, I. A. A finite volume method for computation of fluid flow in complex geometries. Ph.D. thesis, University of London, UK, 1982
22 Lee, S. Y. Flow calculation in a valve/port assembly. M.Sc. thesis, National Chiao Tung University, Taiwan, 1991

Appendix: Calculation of face velocities

For a control volume surrounding a node P considered in Figure 2 the discretized momentum equations for the velocities u and v can be obtained, with the use of the method described in the section titled Numerical solution procedure.

$$u_P = H(u_C) + D_u(p_e - p_w) + E_u(p_n - p_s) + S_u \quad \text{(A1)}$$

$$v_P = H(v_C) + D_v(p_e - p_w) + E_v(p_n - p_s) + S_v \quad \text{(A2)}$$

The terms $H(u_c)$ and $H(v_c)$ denote the effects of neighboring points E, W, N, and S via the convective and diffusive fluxes. In the SIMPLE[18] algorithm the velocities on cell faces are required such that the continuity is satisfied for each control volume. To avoid the problem of pressure-velocity decoupling, the discretized momentum equations for the nodes adjacent to the considered face are used as the basis for interpolation. Given as an example, consider the east-face point e (Figure 2). The velocities at this point are calculated in the following manner

$$u_e = \overline{H(u_C)} + \overline{D_u}(p_E - p_P) + \overline{E_u}(p_{ne} - p_{se}) + \overline{S_u} \quad \text{(A3)}$$

$$v_e = \overline{H(v_C)} + \overline{D_v}(p_E - p_P) + \overline{E_v}(p_{ne} - p_{se}) + \overline{S_v} \quad \text{(A4)}$$

In these equations the terms and coefficients with overbars are obtained through liner interpolation of the corresponding parts in the momentum equations for nodes P and E as given by Equations A1 and A2. The pressure gradients are approximated by central difference. In the equations P_{ne} and P_{se} are the pressures at the cell vertices *ne* and *se* (Figure 2) and can be estimated through interpolation from the neighboring nodal values. In order to ensure continuity constraint and derive a pressure correction equation, the velocities are related to the pressure as, following the SIMPLE algorithm,

$$u'_P = D_u(p'_e - p'_w) + E_u(p'_n - p'_s) \quad (16)$$

$$v'_P = D_v(p'_e - p'_w) + E_v(p'_n - p'_s) \quad (17)$$

where the superscript ′ denotes corrections. Similarly, for the face velocities,

$$u'_e = \overline{D_u}(p'_E - p'_P) + \underline{\overline{E_u}(p'_{ne} - p'_{se})} \quad (18)$$

$$v'_e = \overline{D_v}(p'_E - p'_P) + \underline{\overline{E_v}(p'_{ne} - p'_{se})} \quad (19)$$

The underlined terms are neglected in the solution iteration. This simplification is justifiable mainly based on the assumption that the final solution would not change as long as the solution process converges.